IECE

IECE Transactions on Internet of Things
http://dx.doi.org/10.62762/TIOT.2024.682080

RESEARCH ARTICLE

Advancements in Multi-Year Ice Concentration Estimation from SSM/I 91.6GHz Observations

Yue Zhao[1,*], **Xingdong Wang**[1] **and Zifan Zhang**[1]

[1] College of Information Science and Engineering, Henan University of Technology, Zhengzhou 450001, China

Abstract

To enhance the LOMAX algorithm for sea ice concentration analysis in the polar regions, SSM/I 91.6GHz data was utilized, addressing the underuse of higher frequency data. The refinement process involved redefining PCT values for one-year and multi-year ice regions through both interpolation and least squares methods. Moreover, band operations were conducted to facilitate Arctic multi-year ice concentration retrieval. Comparative analyses with the NT algorithm indicated that the Arctic sea ice extents determined by both algorithms were similar, affirming the credibility of the modified LOMAX algorithm. When examining the results for March and September, the updated LOMAX algorithm demonstrated improved accuracy over the NT algorithm, especially under summer ice melt conditions, highlighting the enhanced performance and reliability of the refined algorithm in various seasonal contexts.

Keywords: LOMAX, Multi-year ice concentration, 91.6 GHz.

Citation
Zhao, Y., Wang, X., & Zhang, Z. (2024). Advancements in Multi-Year Ice Concentration Estimation from SSM/I 91.6GHz Observations. IECE Transactions on Internet of Things, 2(1), 26–35.

Academic Editor:
Jinchao Chen

Submitted: 15 January 2024
Accepted: 27 February 2024
Published: 12 March 2024

Vol. 2, **No.** 1, 2024.
10.62762/TIOT.2024.682080

***Corresponding author:**
✉ Yue Zhao
ZhaoY91028@hotmail.com

1 Introduction

Sea ice is integral to the climate system, primarily due to its high albedo compared to water, which significantly affects the radiation balance at the ocean surface and modulates the heat exchange between the sea surface and the atmosphere. Furthermore, the formation of sea ice is crucial for the development of deep ocean water, thereby influencing ocean circulation and climate change. Arctic sea ice can be classified into one-year ice and multi-year ice. One-year ice lasts no more than a year, melting during the subsequent melting season, while multi-year ice persists for more than one year after the melt season. The sum of one-year ice and multi-year ice constitutes the total sea ice. These ice types differ in thickness, structure, salinity, and albedo, as well as in the heat exchange between the ocean surface and the atmosphere. The distribution trend of one-year ice serves as an indicator of climate change: rising temperatures lead to a decrease in one-year ice distribution, and vice versa. Consequently, it is essential to calculate the concentrations of multi-year and one-year ice separately.

In the realm of sea ice concentration inversion algorithm research, Cavalieri et al. utilized 19.4GHz vertical and horizontal polarization brightness temperature data alongside 37GHz vertical polarization brightness temperature data from the Scanning Multichannel Microwave Radiometer (SMMR) to develop the NASA Team algorithms for retrieving one-year and multi-year ice concentrations [1]. COMISO built on this by using similar data to develop the Bootstrap algorithm, which is based on the fundamental energy transport equation and varying sea ice emissivity characteristics across different frequency bands [2]. Markus et al. further enhanced the NASA Team algorithm, leading to the creation of the NASA Team2 algorithm by incorporating

89GHz vertical and horizontal polarization brightness temperature data [3]. Hao improved the accuracy of multi-year ice concentration by integrating AMSR-E 6.9 GHz data into the existing NASA Team algorithm [4]. Lomax et al. introduced the LOMAX algorithm for retrieving sea ice concentration using SSM/I 85.5GHz data, leveraging the polarization-corrected brightness temperature concept [5]. Kern et al. devised a new method to enhance sea ice concentration inversion accuracy by analyzing the impact of melt ponds on microwave brightness temperature and sea ice concentration results during summer [6]. Korosov et al. proposed a method for estimating sea ice distribution across different ice ages [7]. Gabarro et al. combined maximum likelihood with brightness temperature difference to estimate Arctic sea ice concentration [8]. Ye et al. incorporated air temperature data to improve sea ice concentration accuracy [9]. Zhang et al. developed a double polarization ratio algorithm for retrieving sea ice concentration using 36.5GHz band data and further refined this algorithm [10]. Wang Huanhuan presented a method for inverting multi-year ice concentration based on 89GHz band brightness temperature data and the differing characteristics of one-year ice, multi-year ice, and seawater [11]. Zhang Xiang et al. utilized HY-2 satellite microwave radiometer data to retrieve polar sea ice concentration [12]. Shi Lijian et al. applied HY-2 satellite microwave radiometer data to retrieve Arctic sea ice concentration based on the NASA Team algorithm [13]. Song Xiangyu et al. introduced a fully constrained least squares method to estimate sea ice concentration by incorporating brightness temperature polarization gradient rate and spectral gradient rate [14].

In this paper, we redefined the connection point value in the LOMAX algorithm using higher resolution SSM/I 91.6GHz data. This refinement allowed us to derive the new Arctic multi-year ice range through the sea ice concentration inversion formula. Comparative analysis with the NASA Team algorithm's inversion results indicates that our proposed algorithm achieves higher accuracy and demonstrates feasibility. This study underscores the importance of using high-resolution data for improving the precision of sea ice concentration inversion algorithms, particularly under varying climatic conditions.

2 Study Area and Data

2.1 Overview of the Arctic

The North Pole generally refers to the expansive region located north of 66° 34'N, known as the Arctic Circle. This area encompasses the Arctic Ocean, numerous islands, and portions of the surrounding continents. The Arctic Ocean itself covers an area of approximately 9.5 $\times 106 km^2$, while the combined area of the Arctic lands and islands is about $8 \times 106 km^2$. Notably, about 30% of the world's sea ice is concentrated in this region. The Arctic's unique geographical position has created a distinct natural environment that has been the subject of extensive study by many scholars [15–18].

For the purpose of discussion and analysis, the Arctic region is typically divided into nine distinct sea areas: the Central Arctic Ocean, the Canadian Archipelago, the Greenland Sea, the Sea of Okhotsk, Baffin Bay and the Labrador Sea, the Bering Sea, Hudson Bay, the Kara Sea, and the Barents Sea [14]. Each of these sea areas possesses unique characteristics and plays a significant role in the Arctic's overall environmental and climatic dynamics.

The Central Arctic Ocean, for instance, is the core area of the Arctic and is primarily covered by perennial sea ice. The Canadian Archipelago, located to the north of Canada, consists of numerous islands and channels, which are often navigable only during the summer months due to ice coverage. The Greenland Sea, situated between Greenland and Svalbard, is a critical area for sea ice formation and melting processes. The Sea of Okhotsk, located to the west of the Kamchatka Peninsula, is influenced by both Arctic and Pacific climatic conditions.

Baffin Bay and the Labrador Sea, located between Greenland and Canada, serve as significant conduits for the movement of sea ice between the Arctic and the North Atlantic. The Bering Sea, between Alaska and Russia, acts as a gateway between the Arctic and Pacific Oceans. Hudson Bay, located in northeastern Canada, experiences extensive seasonal ice cover and has a unique hydrological and climatic regime. The Kara Sea, to the north of Siberia, and the Barents Sea, to the north of Norway and Russia, are critical regions for studying the interactions between sea ice, ocean currents, and atmospheric conditions.

In conclusion, the Arctic region's division into these nine sea areas facilitates detailed and focused research on its complex and dynamic natural environment. Understanding the unique characteristics and

interactions within these areas is essential for comprehending the broader implications of Arctic changes on global climate systems.

2.2 Data source

This article utilizes brightness temperature data on sea ice sourced from the National Snow and Ice Data Center (NSIDC), which collaborates with NASA to provide comprehensive polar sea ice, glacier, and snow cover data. The data employed in this study is primarily derived from the original brightness and polarization data collected by various microwave radiometers. These radiometers include the Scanning Multi-Frequency Microwave Radiometer (SSMR) onboard the Nimbus-7 satellite, as well as the multi-band Microwave Imager (Special Sensor Microwave Imager, SSM/I) and the Special Sensor Microwave Imager Sounder (SSMIS) carried by the Defense Meteorological Satellite Program (DMSP) satellites F8, F11, F13, and F17 of the United States.

The SSMR generates data every other day, while the SSM/I and SSMIS provide daily data. Table 1 lists the operational and service periods for each sensor. The NSIDC offers two main datasets for sea ice concentration: the NT dataset, derived using the NASA Team algorithm, and the BS dataset, obtained using the Bootstrap algorithm.

The SSMR, SSM/I, and SSMIS sensors play a crucial role in monitoring and analyzing sea ice conditions. The SSMR, with its ability to measure at multiple frequencies, provides valuable data every other day, allowing researchers to track changes in sea ice over time. The SSM/I and SSMIS sensors, with their daily data generation, offer higher temporal resolution, which is essential for capturing rapid changes in sea ice dynamics.

In this study, the brightness temperature data from these sensors are analyzed to gain insights into sea ice concentration and distribution. The NT dataset, based on the NASA Team algorithm, utilizes specific microwave frequencies to estimate sea ice concentration by distinguishing between different types of surfaces, such as open water, first-year ice, and multi-year ice. Similarly, the BS dataset, derived from the Bootstrap algorithm, employs a different set of microwave frequencies and algorithms to estimate sea ice concentration with high accuracy.

By leveraging these datasets, we can obtain a comprehensive understanding of sea ice conditions in the polar regions. The data allows for the examination of seasonal and interannual variations in sea ice extent, as well as the assessment of long-term trends related to climate change. The integration of brightness temperature data with advanced algorithms provides a robust framework for accurately monitoring and predicting sea ice dynamics, which is crucial for climate research and the development of effective mitigation strategies.

In summary, the brightness temperature data from NSIDC, combined with the NASA Team and Bootstrap algorithms, provide invaluable resources for studying sea ice. These datasets enable detailed analysis of sea ice concentration and dynamics, contributing to our understanding of polar environments and their response to changing climatic conditions.

Table 1. Describes the running time of SSM/I (SSMR and SSMIS) sensors.

satellite	sensor	run time
Nimbus-7	SSMR	1978-1987
DMSP F8	SSM/I	1987/07/09-1991/12/02
DMSP F11	SSM/I	1991/12/03-1995/09/30
DMSP F13	SSM/I	1995/10/01-2007/12/31
DMSP F17	SSMIS	2008/01/01-now

3 Method

3.1 LOMAX algorithm

In 1995, Lomax et al. proposed an algorithm to calculate the overall sea ice and multi-year ice concentrations using SSM/I 85.5 GHz data. This algorithm is based on the concept of Polarization Corrected Temperature (PCT), introduced by Silence et al. in 1989. PCT accounts for the influence of volume scattering on the brightness temperature observed by satellites and is defined as follows:

$$PCT = \left(\beta T_{bh} - T_{bv}\right) / \left(\beta - 1\right) \tag{1}$$

where T_{bhc} and T_{bvc} represent the brightness temperatures of horizontal and vertical polarization on the cloudless sea observed by satellites, and T_{bho} and T_{bvo} are the brightness temperatures of horizontal and vertical polarization observed on the ocean surface using measurement ships and buoys. The parameter β is used to correct the absorption of gases in the atmosphere, thereby indicating the optical depth of the atmosphere. Silence et al. determined through modeling that, for the dry air over polar regions, the value of β is approximately 0.38.

The specific steps of the LOMAX algorithm for calculating multi-year ice concentration are as follows: first, the PCT of the overall sea ice data is obtained. Next, the polarization correction temperatures of 100% one-year ice (PCT_F) and 100% multi-year ice (PCT_M) are calculated. Using these values, the multi-year ice concentration (C_M) can then be determined as:

$$C_M = C_T \left(\frac{PCT - PCT_F}{PCT_M - PCT_F} \right) \tag{2}$$

While the original LOMAX algorithm is effective, there is potential for improvement in data resolution. To enhance the algorithm, high-resolution data is introduced. The improved algorithm involves first calculating the PCT for 100% one-year ice and 100% multi-year ice, and then retrieving the multi-year ice concentration.

This enhancement allows for more accurate and detailed measurements, improving the ability to monitor and analyze multi-year ice concentration. By using higher resolution data, the refined algorithm can better capture subtle variations and provide more precise estimates of ice distribution. This improvement is crucial for understanding the dynamics of sea ice and its response to climatic changes.

In summary, the improved LOMAX algorithm, which integrates high-resolution data, offers a significant advancement over the original method. It provides a more detailed and accurate assessment of multi-year ice concentration, enhancing our ability to monitor sea ice conditions and contributing to better-informed climate research and policy decisions.

3.2 Multi-year ice concentration retrieval based on 91.6 GHz

Firstly, radiometric correction, masking, and radiometric calibration were applied to the SSM/I 91.6 GHz vertical and horizontal brightness temperature data. Following this, polarization values were computed by processing the vertical and horizontal brightness temperature data for the year 2017, leading to the calculation of the polarization correction temperature (PCT). Given that the NASA Team algorithm is capable of retrieving both multi-year and one-year ice concentrations, this study initially compares the inversion performance results of the NASA Team algorithm with the PCT values. Through statistical analysis, the least squares method, and linear analysis, we derived the PCT values for regions with 100% multi-year ice and 100% one-year ice. However, because the multi-year ice concentration calculated by the NASA Team algorithm is based on low-frequency data, and the PCT value is derived from 91.6 GHz high-frequency data, resampling using the nearest neighbor method was necessary.

Next, the multi-year ice concentration at each point was inversely calculated using the LOMAX algorithm. The inversion results were then compared with the multi-year ice retrieval results obtained by the NASA Team algorithm. The specific research steps are outlined as follows:

3.3 Data Processing

Initially, the 91.6 GHz vertical and horizontal brightness temperature data were acquired, followed by the application of radiometric correction to enhance the brightness temperature data. The band operation formula used is as follows:

$$b_3 = float\left(b_1\right)/10 * 1.0286 - 3.0094 \tag{3}$$

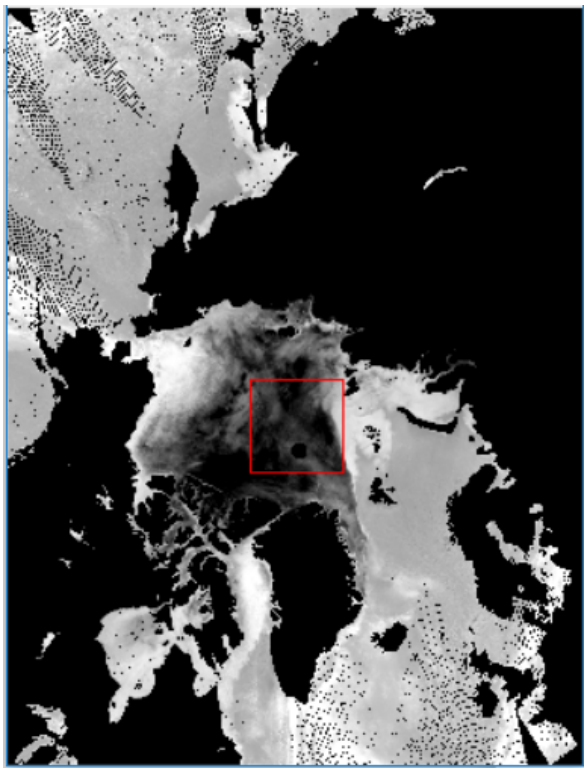

Figure 1. After brightness temperature treatment.

Given that our analysis focuses on sea ice over the ocean, it was essential to mask the data to remove land interference. In the NSIDC dataset, a data value of 1 denotes land, while 0 denotes the ocean. However, for our purposes, we needed the data value to be 1 for the ocean and 0 for land. The necessary band operations are outlined in Formula (4), where "eq" represents

equality, and "ne" denotes inequality, followed by the masking operation in Formula (5). The processed image is illustrated in Figure 1.

$$b_3 = (b_1 eq1) * 0 + (b_1 ne1) * 1 \quad (4)$$

$$b_4 = b_1 * b_2 \quad (5)$$

3.4 Obtaining the New Polarization Correction Temperature (PCT) Value

According to the LOMAX algorithm, PCT is defined as:

$$PCT = (\beta T_{bh} - T_{bv}) / (\beta - 1) \quad (6)$$

Where β is 0.38. The band operation formula for generating PCT data is shown in Formula (**??**). The resulting PCT image is displayed in Figure 2, where each point corresponds to the polarization corrected temperature (PCT) value. Compared to the original brightness temperature image, the PCT image exhibits significantly reduced noise. The polarization corrected temperature offers two main advantages: it eliminates atmospheric errors, water vapor, and cloud effects, regardless of the weather, and it amplifies the distinction between multi-year ice and one-year ice, facilitating the determination of system point values.

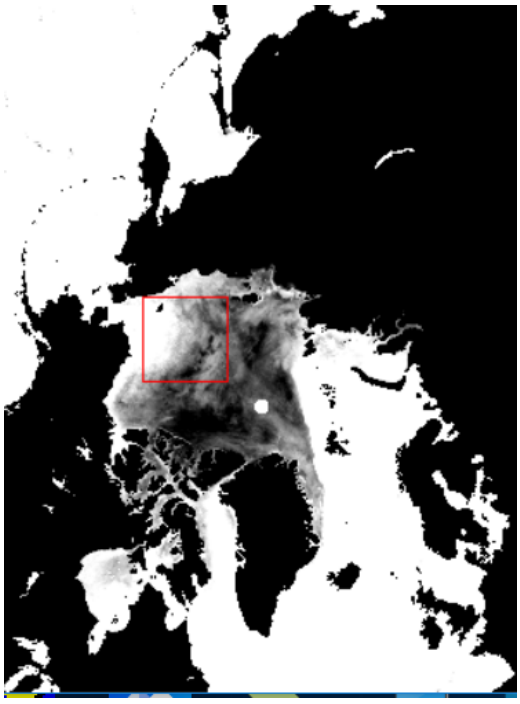

Figure 2. Data graph of PCT values.

3.5 Determination of Core Parameters

During September, there is more multi-year ice and open water, with less one-year ice. Consequently, the selection period for multi-year ice ranges from January to May and November to December. The latitude range for selecting multi-year ice in the specified area is $76° - 78°$ North, and the longitude range is $77° - 79°$ East. For September, multi-year ice was selected between $84° - 86°$ North. Refer to Figure 3. Based on the statistics of PCT values for 50 points with multi-year ice concentration greater than 0.8 in this region, a linear decreasing relationship between multi-year ice concentration and PCT value is observed. Using the least squares method, the slope k of the linear equation is -144.45, and the intercept B is 322.06. It can be inferred that the PCT value of 100% multi-year ice is approximately 201.837.

Determining the PCT value for 100% one-year ice is more challenging, as one-year ice areas can also contain multi-year ice. Therefore, regions with high one-year ice concentration and no multi-year ice must be selected. Typically, there is very little one-year ice in the summer. Hence, it is necessary to select the one-year ice concentration at a specific location and then infer the area with 100% one-year ice concentration.

The multi-year ice area in September was selected to analyze the relationship between multi-year ice concentration and PCT value. To remove the influence of multi-year ice, the PCT value can be corrected by accounting for the influence factors of multi-year ice removal. The formula is as follows, where C_M is multi-year ice concentration and C_F is one-year ice concentration. This formula assumes that the multi-year ice area behaves like open water, eliminating the impact of one-year ice. By using ENVI software to find the average PCT values for open water areas, the corrected PCT value for open water is approximately 269.837. The resulting formula is shown in Formula (7). Finally, the relationship between multi-year ice and corrected brightness temperature is illustrated in Figures 4 and 5. The polarization corrected temperature PCT for the 100% one-year ice region is determined to be 251.244.

$$b_1 = PCT - 269.837 * (1 - C_F - C_M) \quad (7)$$

The retrieval formula for the multi-year ice algorithm is obtained once the system point values of the LOMAX algorithm are determined. The band operation formula is as follows: b_2 represents the known sea ice density result graph, and b_3 is the known PCT data graph.

$$b_1 = b_2 \left(\frac{b_3 - 251.244}{201.837 - 251.244} \right) \quad (8)$$

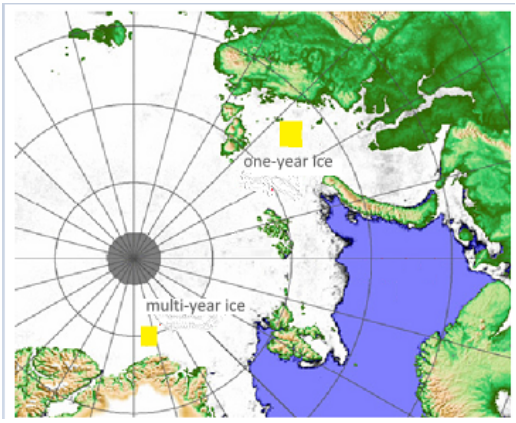

Figure 3. Selected areas of multi-year and one-year ice.

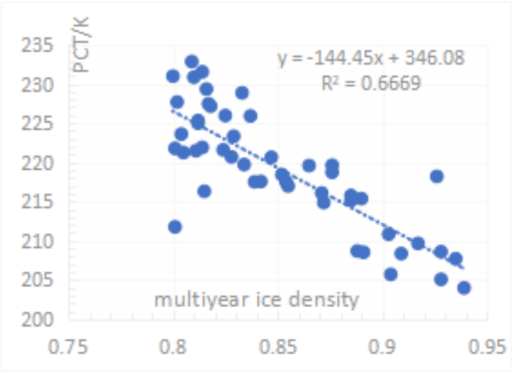

Figure 4. Relationship between multi-year ice concentration and PCT value.

4 Results and Analysis

Based on the brightness temperature data of 91.6GHz vertical and horizontal polarization, this study corrected the LOMAX algorithm to derive the retrieval formula for multi-year ice concentration and subsequently generated the multi-year ice concentration data graph. March and September represent the months with the maximum and minimum Arctic sea ice extents, respectively. The results obtained in this study were compared with those derived from the NASA Team algorithm for multi-year ice concentration for March, September, and the entire year of 2017.

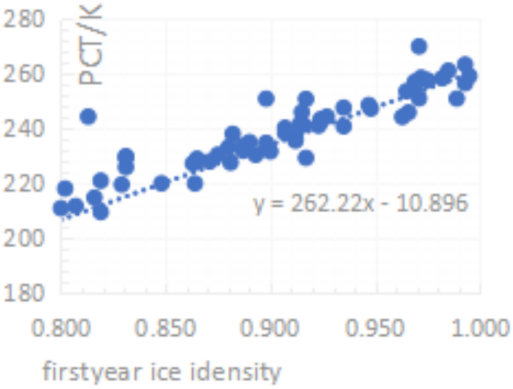

Figure 5. Relationship between one-year ice concentration and corrected PCT value.

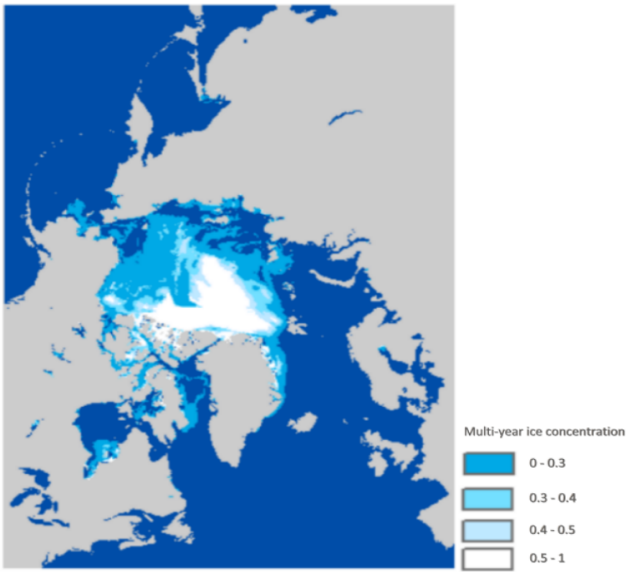

(a) Using the improved LOMAX algorithm for multi-year ice inversion

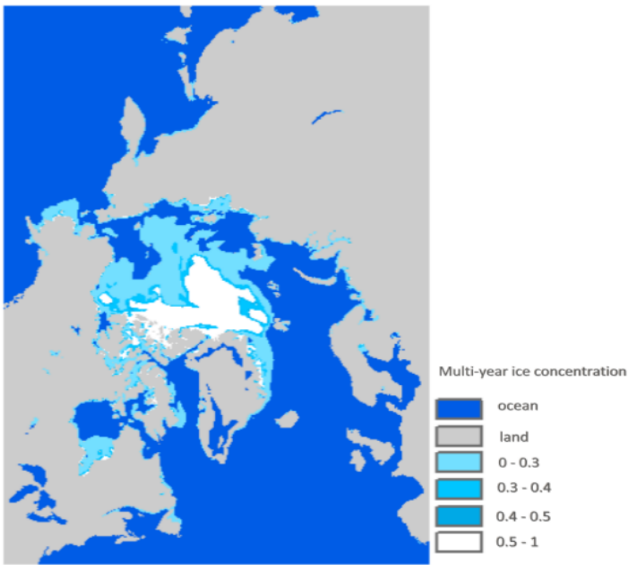

(b) Multi-year ice retrieval using NASA Team algorithms

Figure 6. Comparison of multi-year ice concentration in March 2017.

In March, the area with a multi-year ice concentration greater than 0.5, as calculated by the modified LOMAX algorithm, was approximately 1.64×10^6 km^2, whereas the NASA Team algorithm estimated this area to be about 1.55×10^6 km^2. The difference in area is around 9×10^4 km^2, which is relatively minor. However, for regions with multi-year ice concentrations between 0 and 0.5, the modified LOMAX algorithm calculated an area of about 6.44×10^6 km^2, while the NASA Team algorithm estimated approximately 5.73×10^6 km^2.

This results in a difference of about 7.1 $\times$ 10^5 km^2. As illustrated in Figure 6, the discrepancy between the two algorithms is mainly found near the coastlines of the Chukchi Sea and the East Siberian Sea, where the concentration is less than 0.5.

The difference map for March was generated using band operations and color matching. By subtracting the multi-year ice concentration map obtained by the NASA Team algorithm from the one derived using the modified LOMAX algorithm, the difference map shown in Figure 7 was produced. Compared to the NASA Team algorithm, the area with a higher concentration is about 4.34 $\times$ 10^6 km^2, while the area with a lower concentration is about 2.55 $\times$ 10^6 km^2. The absolute value of the concentration difference at each point was calculated, yielding a final average value of approximately 0.141. This indicates that there is a noticeable, though not substantial, difference in concentration between the LOMAX and NASA Team algorithm results for March 2017. In mid-March, the average multi-year ice concentration and the area with a multi-year ice concentration greater than 0, as derived by the LOMAX algorithm, are larger than those retrieved by the NASA Team algorithm. Potential reasons for this include the influence of snow and weather. High-frequency data, while offering higher resolution, is more susceptible to weather-related interference, which is difficult to completely eliminate even with weather filters. The cold temperatures in March can cause interference from cold air, atmosphere, and clouds, leading to lower brightness temperature values, subsequently resulting in lower polarization correction temperature values and higher estimated multi-year ice concentrations.

Overall, the comparison of inversion results between the two algorithms for March shows that the modified LOMAX algorithm generally estimates larger areas with concentrations greater than 0, but the differences are not significant, and the areas with multi-year ice density greater than 0.5 are quite similar. The average concentration difference at each point in March is about 0.141.

For the September results, a similar analysis was conducted. Figure 8 shows the multi-year ice concentration maps obtained using both the modified LOMAX algorithm and the NASA Team algorithm. In September, the area with a multi-year ice concentration greater than 0.5 was estimated to be 1.69 $\times$ 10^6 km^2 by the modified LOMAX algorithm and 2.07 $\times$ 10^6 km^2 by the NASA Team algorithm, resulting

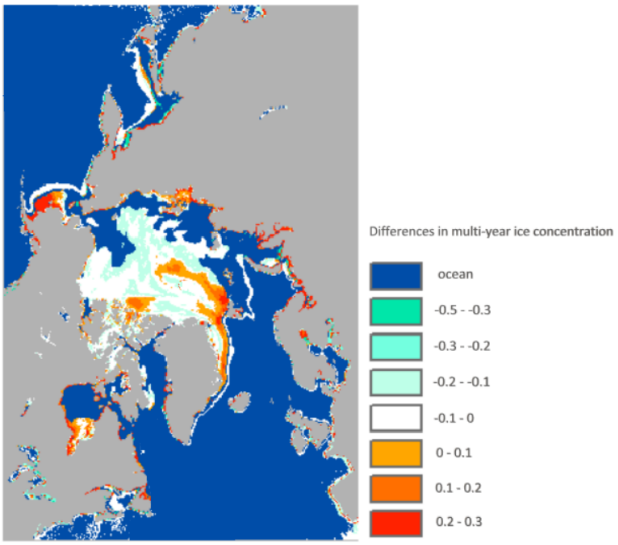

Figure 7. Multi-year ice concentration differences in March 2017.

in a 22% difference. Unlike March, the multi-year ice concentration greater than 0.5 retrieved by the modified LOMAX algorithm is smaller than that retrieved by the NASA Team algorithm. This may indicate that high-frequency data accuracy is influenced by atmospheric conditions, temperature, and clouds. For areas with a multi-year ice concentration greater than 0, the results from both algorithms are 3.72 $\times$ 10^6 km^2 (modified LOMAX) and 3.89 $\times$ 10^6 km^2 (NASA Team), respectively, showing a minor difference of about 4%. This suggests that while there is minimal difference in the areas with a multi-year ice concentration greater than 0 in September, there is a notable difference in the areas with concentrations greater than 0.5. This indicates that the modified LOMAX algorithm can accurately determine the range of multi-year ice, but further refinement is needed for accurately retrieving multi-year ice concentrations.

The difference map for September, shown in Figure 9, was created using band operations. It reveals that the multi-year ice concentration retrieved by the NASA Team algorithm is larger in most Arctic regions than that obtained using the modified LOMAX algorithm, covering an area of about 2.1 $\times$ 10^6 km^2. Conversely, the modified LOMAX algorithm yields higher multi-year ice concentrations in the northwest part of Greenland, while the NASA Team algorithm shows higher concentrations in other regions. The average absolute difference in multi-year ice concentration at each point is about 0.25, indicating a noticeable difference that warrants further refinement of the retrieval algorithm. Nonetheless,

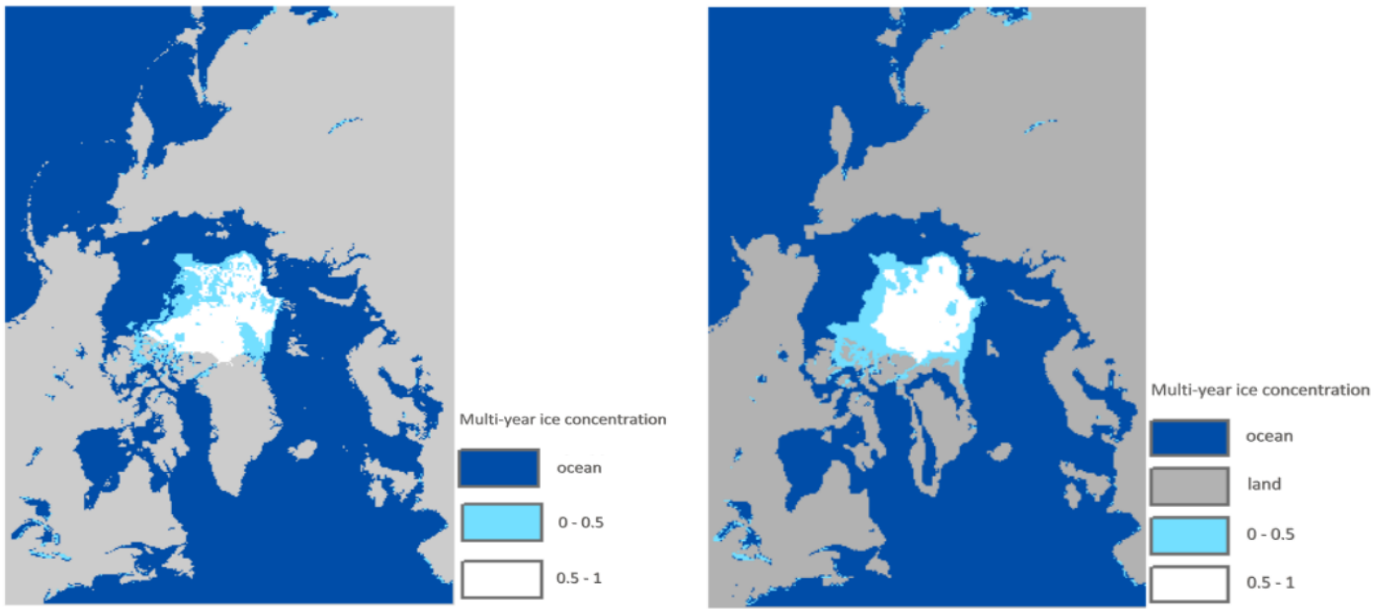

(a) Using the improved LOMAX algorithm for multi-year ice retrieval

(b) Multi-year ice retrieval using NASA Team algorithms

Figure 8. Comparison of multi-year ice concentration in September 2017.

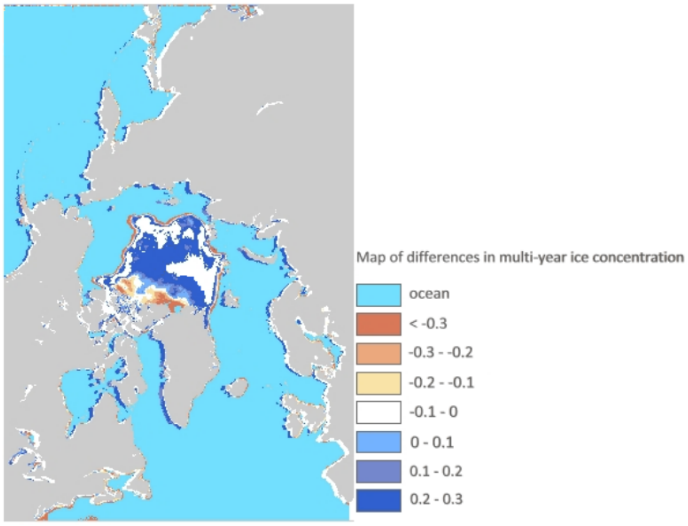

Figure 9. Comparison difference of multi-year ice concentration in September 2017.

the distribution range of areas with multi-year ice concentrations greater than 0 is quite similar between the two methods. Thus, based on the 91.6GHz data, the modified LOMAX algorithm effectively determines the range of multi-year ice, although the specific concentration estimates need further improvement.

To further verify the accuracy of the algorithm after modifying the system point values, the average multi-year ice concentration for 2017 obtained using both algorithms was compared, as shown in Figure 9. The area with a multi-year ice concentration greater than 0 retrieved by the modified LOMAX algorithm is about 4.60×10^6 km^2 (Figure 9a), while the NASA Team algorithm estimates it to be 4.35×10^6 km^2 (Figure 9b). This area difference of only 5.4% suggests that the retrieval algorithm and coefficients used in this study are feasible for determining the distribution range of multi-year ice. For regions with a multi-year ice concentration greater than 0.3, the areas retrieved by the two algorithms are 1.96×10^6 km^2 and 2.22×10^6 km^2, respectively, with an 11% difference. This indicates that there is minimal discrepancy between the two algorithms for regions with multi-year ice concentrations between 0 and 0.3.

5 Conclusion

The high resolution and frequency of passive microwave radiometer SSM/I data have not been fully leveraged in the study of multi-year ice concentration within sea ice research. Applying the LOMAX sea ice concentration retrieval algorithm to high-frequency data is a valuable research direction, and verifying the algorithm's accuracy is crucial. This study compares the sea ice concentration obtained using the NASA Team retrieval algorithm with results from the LOMAX algorithm, enhancing the validation of existing methods. Results show minimal differences in sea ice extent, confirming the feasibility of the proposed algorithm. During summer, surface melting introduces uncertainty, but this algorithm yields more accurate results than the original LOMAX and NASA

Team (NT) algorithms, which are influenced by ice-to-snow emissivity ratios. Future research should address the algorithm's performance across different regions, weather conditions, and sea ice surfaces, and examine the impact of system point value selection on inversion results, ensuring robust and precise sea ice concentration retrieval under diverse conditions.

Conflicts of Interest

The authors declare that they have no conflicts of interest.

Acknowledgement

This work was supported without any funding.

References

[1] Cavalieri D J. (1994). A microwave technique for mapping thin sea ice[U]. *Journal of Geophysical Research Oceans*. 99(C6):12561-12572. [CrossRef]

[2] Cavalieri, D. J., Gloersen, P., & Campbell, W. J. (1984). Determination of sea ice parameters with the Nimbus 7 SMMR. *Journal of Geophysical Research: Atmospheres*, 89(D4), 5355-5369. [CrossRef]

[3] Cavalieri, D. J., & Parkinson, C. L. (2012). Arctic sea ice variability and trends, 1979–2010. *The Cryosphere*, 6(4), 881-889. [CrossRef]

[4] Comiso, J. C., & Nishio, F. (2008). Trends in the sea ice cover using enhanced and compatible AMSR-E, SSM/I, and SMMR data. *Journal of Geophysical Research: Oceans*, 113(C2). [CrossRef]

[5] Comiso, J. C. (1986). Characteristics of Arctic winter sea ice from satellite multispectral microwave observations. Journal of Geophysical Research: Oceans, 91(C1), 975-994. [CrossRef]

[6] Ulaby, F. T., Kouyate, F., Brisco, B., & Williams, T. L. (1986). Textural infornation in SAR images. *IEEE Transactions on Geoscience and Remote Sensing*, (2), 235-245. [CrossRef]

[7] Soh, L. K., Tsatsoulis, C., Gineris, D., & Bertoia, C. (2004). ARKTOS: An intelligent system for SAR sea ice image classification. *IEEE Transactions on geoscience and remote sensing*, 42(1), 229-248. [CrossRef]

[8] Ressel, R., Frost, A., & Lehner, S. (2015). A neural network-based classification for sea ice types on X-band SAR images. *IEEE Journal of Selected Topics in Applied Earth Observations and Remote Sensing*, 8(7), 3672-3680. [CrossRef]

[9] Cavalieri, D. J., Parkinson, C. L., Gloersen, P., Comiso, J. C., & Zwally, H. J. (1999). Deriving long-term time series of sea ice cover from satellite passive-microwave multisensor data sets. *Journal of Geophysical Research: Oceans*, 104(C7), 15803-15814. [CrossRef]

[10] Nghiem, S. V., Steffen, K., Kwok, R., & Tsai, W. Y. (2001). Detection of snowmelt regions on the Greenland ice sheet using diurnal backscatter change. *Journal of Glaciology*, 47(159), 539-547. [CrossRef]

[11] Gough, S. R. (1972). A low temperature dielectric cell and the permittivity of hexagonal ice to 2 K. *Canadian Journal of Chemistry*, 50(18), 3046-3051. [CrossRef]

[12] Li, Y., & Cao, J. (2023). Adaptive Binary Particle Swarm Optimization for WSN Node Optimal Deployment Algorithm. *IECE Transactions on Internet of Things*, 1(1), 1-8. [CrossRef]

[13] Spreen, G., Kaleschke, L., & Heygster, G. (2008). Sea ice remote sensing using AMSR-E 89-GHz channels. *Journal of Geophysical Research: Oceans*, 113(C2). [CrossRef]

[14] Y. Hua & X. Wang (2023). Forest Fire Assessment and Analysisin Liangshan, Sichuan Province Based on Remote Sensing. *IECE Transactions on Internet of Things*, 1(1), 15–21. [CrossRef]

[15] Lv, Y., Fang, F. A. N. G., Yang, T., & Romero, C. E. (2020). An early fault detection method for induced draft fans based on MSET with informative memory matrix selection. *ISA transactions*, 102, 325-334. [CrossRef]

[16] Fang, F. A. N. G., Tan, W., & Liu, J. Z. (2005). Tuning of coordinated controllers for boiler-turbine units. *Acta Automatica Sinica*, 31(2), 291-296.

[17] Fang, F., Jizhen, L., & Wen, T. (2004). Nonlinear internal model control for the boiler-turbine coordinate systems of power unit. *PROCEEDINGS-CHINESE SOCIETY OF ELECTRICAL ENGINEERING*, 24(4), 195-199.

[18] Wang, N., Fang, F., & Feng, M. (2014, May). Multi-objective optimal analysis of comfort and energy management for intelligent buildings. In *The 26th Chinese control and decision conference (2014 CCDC)* (pp. 2783-2788). IEEE.

Yue Zhao Currently majoring in electronic Information in College of Information Science and Engineering, Henan University of Technology. The research direction is remote sensing in sea ice concentration.

Xingdong Wang Currently working at the School of Information Science and Engineering, Henan University of Technology. His current research interests include remote sensing, GIS(geographic information system).

Zifan Zhang From 2016 to 2020, he graduated from the computer department of Henan University of technology with a bachelor's degree. His research interests is Spatial information and digital technology.